

Measurement of vector boson plus $D^*(2010)^+$ meson production in $\bar{p}p$ collisions at $\sqrt{s} = 1.96$ TeV

T. Aaltonen,²¹ S. Amerio,^{39a,39b} D. Amidei,³¹ A. Anastassov,^{15,w} A. Annovi,¹⁷ J. Antos,¹² G. Apollinari,¹⁵ J. A. Appel,¹⁵ T. Arisawa,⁵² A. Artikov,¹³ J. Asaadi,⁴⁷ W. Ashmanskas,¹⁵ B. Auerbach,² A. Aurisano,⁴⁷ F. Azfar,³⁸ W. Badgett,¹⁵ T. Bae,²⁵ A. Barbaro-Galtieri,²⁶ V. E. Barnes,⁴³ B. A. Barnett,²³ P. Barria,^{41a,41c} P. Bartos,¹² M. Baucus,^{39a,39b} F. Bedeschi,^{41a} S. Behari,¹⁵ G. Bellettini,^{41a,41b} J. Bellinger,⁵⁴ D. Benjamin,¹⁴ A. Beretvas,¹⁵ A. Bharti,⁴⁵ K. R. Bland,⁵ B. Blumenfeld,²³ A. Bocci,¹⁴ A. Bodek,⁴⁴ D. Bortoletto,⁴³ J. Boudreau,⁴² A. Boveia,¹¹ L. Brigliadori,^{6a,6b} C. Bromberg,³² E. Brucken,²¹ J. Budagov,¹³ H. S. Budd,⁴⁴ K. Burkett,¹⁵ G. Busetto,^{39a,39b} P. Bussey,¹⁹ P. Butti,^{41a,41b} A. Buzatu,¹⁹ A. Calamba,¹⁰ S. Camarda,⁴ M. Campanelli,²⁸ F. Canelli,^{11,ee} B. Carls,²² D. Carlsmith,⁵² R. Carosi,^{41a} S. Carrillo,^{16,1} B. Casal,^{9,j} M. Casarsa,^{48a} A. Castro,^{6a,6b} P. Catastini,²⁰ D. Cauz,^{48a,48b,48c} V. Cavaliere,²² A. Cerri,^{26,e} L. Cerrito,^{28,r} Y. C. Chen,¹ M. Chertok,⁷ G. Chiarelli,^{41a} G. Chlachidze,¹⁵ K. Cho,²⁵ D. Chokheli,¹³ A. Clark,¹⁸ C. Clarke,⁵³ M. E. Convery,¹⁵ J. Conway,⁷ M. Corbo,^{15,z} M. Cordelli,¹⁷ C. A. Cox,⁷ D. J. Cox,⁷ M. Cremonesi,^{41a} D. Cruz,⁴⁷ J. Cuevas,^{9,y} R. Culbertson,¹⁵ N. d'Ascenzo,^{15,v} M. Datta,^{15,hh} P. de Barbaro,⁴⁴ L. Demortier,⁴⁵ M. Deninno,^{6a} M. D'Errico,^{39a,39b} F. Devoto,²¹ A. Di Canto,^{41a,41b} B. Di Ruzza,^{15,p} J. R. Dittmann,⁵ S. Donati,^{41a,41b} M. D'Onofrio,²⁷ M. Dorigo,^{48a,48d} A. Driutti,^{48a,48b,48c} K. Ebina,⁵² R. Edgar,³¹ A. Elagin,⁴⁷ R. Erbacher,⁷ S. Errede,²² B. Esham,²² S. Farrington,³⁸ J. P. Fernández Ramos,²⁹ R. Field,¹⁶ G. Flanagan,^{15,t} R. Forrest,⁷ M. Franklin,²⁰ J. C. Freeman,¹⁵ H. Frisch,¹¹ Y. Funakoshi,⁵² C. Galloni,^{41a,41b} A. F. Garfinkel,⁴³ P. Garosi,^{41a,41c} H. Gerberich,²² E. Gerchtein,¹⁵ S. Giagu,^{46a} V. Giakoumopoulou,³ K. Gibson,⁴² C. M. Ginsburg,¹⁵ N. Giokaris,³ P. Giromini,¹⁷ V. Glagolev,¹³ D. Glenzinski,¹⁵ M. Gold,³⁴ D. Goldin,⁴⁷ A. Golossanov,¹⁵ G. Gomez,⁹ G. Gomez-Ceballos,³⁰ M. Goncharov,³⁰ O. González López,²⁹ I. Gorelov,³⁴ A. T. Goshaw,¹⁴ K. Goulianos,⁴⁵ E. Gramellini,^{6a} C. Grosso-Pilcher,¹¹ R. C. Group,^{51,15} J. Guimaraes da Costa,²⁰ S. R. Hahn,¹⁵ J. Y. Han,⁴⁴ F. Happacher,¹⁷ K. Hara,⁴⁹ M. Hare,⁵⁰ R. F. Harr,⁵³ T. Harrington-Taber,^{15,m} K. Hatakeyama,⁵ C. Hays,³⁸ J. Heinrich,⁴⁰ M. Herndon,⁵⁴ A. Hocker,⁴⁷ Z. Hong,^{15,f} W. Hopkins,^{15,f} S. Hou,¹ R. E. Hughes,³⁵ U. Husemann,⁵⁵ M. Hussein,^{32,cc} J. Huston,³² G. Introzzi,^{41a,41e,41f} M. Iori,^{46a,46b} A. Ivanov,^{7,o} E. James,¹⁵ D. Jang,¹⁰ B. Jayatilaka,¹⁵ E. J. Jeon,²⁵ S. Jindariani,¹⁵ M. Jones,⁴³ K. K. Joo,²⁵ S. Y. Jun,¹⁰ T. R. Junk,¹⁵ M. Kambeitz,²⁴ T. Kamon,^{25,47} P. E. Karchin,⁵³ A. Kasmi,⁵ Y. Kato,^{37,n} W. Ketchum,^{11,ii} J. Keung,⁴⁰ B. Kilminster,^{15,ee} D. H. Kim,²⁵ H. S. Kim,^{15,bb} J. E. Kim,²⁵ M. J. Kim,¹⁷ S. H. Kim,⁴⁹ S. B. Kim,²⁵ Y. J. Kim,²⁵ Y. K. Kim,¹¹ N. Kimura,⁵² M. Kirby,¹⁵ K. Knoepfel,¹⁵ K. Kondo,^{52,*} D. J. Kong,²⁵ J. Konigsberg,¹⁶ A. V. Kotwal,¹⁴ M. Kreps,²⁴ J. Kroll,⁴⁰ M. Kruse,¹⁴ T. Kuhr,²⁴ M. Kurata,⁴⁹ A. T. Laasanen,⁴³ S. Lammel,¹⁵ M. Lancaster,²⁸ K. Lannon,^{35,x} G. Latino,^{41a,41c} H. S. Lee,²⁵ J. S. Lee,²⁵ S. Leo,²² S. Leone,^{41a} J. D. Lewis,¹⁵ A. Limosani,^{14,s} E. Lipeles,⁴⁰ A. Lister,^{18,a} H. Liu,⁵¹ Q. Liu,⁴³ T. Liu,¹⁵ S. Lockwitz,⁵⁵ A. Loginov,⁵⁵ D. Lucchesi,^{39a,39b} A. Lucà,¹⁷ J. Lueck,²⁴ P. Lujan,²⁶ P. Lukens,¹⁵ G. Lungu,⁴⁵ J. Lys,²⁶ R. Lysak,^{12,d} R. Madrak,¹⁵ P. Maestro,^{41a,41c} S. Malik,⁴⁵ G. Manca,^{27,b} A. Manousakis-Katsikakis,³ L. Marchese,^{6a,ij} F. Margaroli,^{46a} P. Marino,^{41a,41d} K. Matera,²² M. E. Mattson,⁵³ A. Mazzacane,¹⁵ P. Mazzanti,^{6a} R. McNulty,^{27,i} A. Mehta,²⁷ P. Mehtala,²¹ C. Mesropian,⁴⁵ T. Miao,¹⁵ D. Mietlicki,³¹ A. Mitra,¹ H. Miyake,⁴⁹ S. Moed,¹⁵ N. Moggi,^{6a} C. S. Moon,^{15,z} R. Moore,^{15,ff,gg} M. J. Morello,^{41a,41d} A. Mukherjee,¹⁵ Th. Muller,²⁴ P. Murat,¹⁵ M. Mussini,^{6a,6b} J. Nachtman,^{15,m} Y. Nagai,⁴⁹ J. Naganoma,⁵² I. Nakano,³⁶ A. Napier,⁵⁰ J. Nett,⁴⁷ C. Neu,⁵¹ T. Nigmanov,⁴² L. Nodulman,² S. Y. Noh,²⁵ O. Norniella,²² L. Oakes,³⁸ S. H. Oh,¹⁴ Y. D. Oh,²⁵ I. Oksuzian,⁵¹ T. Okusawa,³⁷ R. Orava,²¹ L. Ortolan,⁴ C. Pagliarone,^{48a} E. Palencia,^{9,e} P. Palmi,³⁴ V. Papadimitriou,¹⁵ W. Parker,⁵⁴ G. Pauletta,^{48a,48b,48c} M. Paulini,¹⁰ C. Paus,³⁰ T. J. Phillips,¹⁴ G. Piacentino,^{15,q} E. Pianori,⁴⁰ J. Pilot,⁷ K. Pitts,²² C. Plager,⁸ L. Pondrom,⁵⁴ S. Poprocki,^{15,f} K. Potamianos,²⁶ A. Pranko,²⁶ F. Prokoshin,^{13,aa} F. Ptohos,^{17,g} G. Punzi,^{41a,41b} I. Redondo Fernández,²⁹ P. Renton,³⁸ M. Rescigno,^{46a} F. Rimondi,^{6a,*} L. Ristori,^{41a,15} A. Robson,¹⁹ T. Rodriguez,⁴⁰ S. Rolli,^{50,h} M. Ronzani,^{41a,41b} R. Roser,¹⁵ J. L. Rosner,¹¹ F. Ruffini,^{41a,41c} A. Ruiz,⁹ J. Russ,¹⁰ V. Rusu,¹⁵ W. K. Sakumoto,⁴⁴ Y. Sakurai,⁵² L. Santi,^{48a,48b,48c} K. Sato,⁴⁹ V. Saveliev,^{15,v} A. Savoy-Navarro,^{15,z} P. Schlabach,¹⁵ E. E. Schmidt,¹⁵ T. Schwarz,³¹ L. Scodellaro,⁹ F. Scuri,^{41a} S. Seidel,³⁴ Y. Seiya,³⁷ A. Semenov,¹³ F. Sforza,^{41a,41b} S. Z. Shalhout,⁷ T. Shears,²⁷ P. F. Shepard,⁴² M. Shimojima,^{49,u} M. Shochet,¹¹ I. Shreyber-Tecker,³³ A. Simonenko,¹³ K. Sliwa,⁵⁰ J. R. Smith,⁷ F. D. Snider,¹⁵ H. Song,⁴² V. Sorin,⁴ R. St. Denis,^{19,*} M. Stancari,¹⁵ D. Stentz,^{15,w} J. Strologas,³⁴ Y. Sudo,⁴⁹ A. Sukhanov,¹⁵ I. Suslov,¹³ K. Takemasa,⁴⁹ Y. Takeuchi,⁴⁹ J. Tang,¹¹ M. Tecchio,³¹ P. K. Teng,¹ J. Thom,¹⁵ E. Thomson,⁴⁰ V. Thukral,⁴⁷ D. Toback,⁴⁷ S. Tokar,¹² K. Tollefson,³² T. Tomura,⁴⁹ D. Tonelli,^{15,e} S. Torre,¹⁷ D. Torretta,¹⁵ P. Totaro,^{39a} M. Trovato,^{41a,41d} F. Ukegawa,⁴⁹ S. Uozumi,²⁵ F. Vázquez,^{16,1} G. Velev,¹⁵ C. Vellidis,¹⁵ C. Vernieri,⁴³ M. Vidal,⁹ R. Vilar,⁹ J. Vizán,^{9,dd} M. Vogel,³⁴ G. Volpi,¹⁷ P. Wagner,⁴⁰ R. Wallny,^{15,j} S. M. Wang,¹ D. Waters,²⁸ W. C. Wester III,¹⁵ D. Whiteson,^{40,c} A. B. Wicklund,² S. Wilbur,⁷ H. H. Williams,⁴⁰ J. S. Wilson,³¹ P. Wilson,¹⁵ B. L. Winer,³⁵ P. Wittich,^{15,f} S. Wolbers,¹⁵ H. Wolfe,³⁵ T. Wright,³¹ X. Wu,¹⁸ Z. Wu,⁵ K. Yamamoto,³⁷ D. Yamato,³⁷ T. Yang,¹⁵ U. K. Yang,²⁵ Y. C. Yang,²⁵ W.-M. Yao,²⁶ G. P. Yeh,¹⁵ K. Yi,^{15,m} J. Yoh,¹⁵ K. Yorita,⁵² T. Yoshida,^{37,k} G. B. Yu,¹⁴ I. Yu,²⁵ A. M. Zanetti,^{48a} Y. Zeng,¹⁴ C. Zhou,¹⁴ and S. Zucchelli,^{6a,6b}

(CDF Collaboration)

¹Institute of Physics, Academia Sinica, Taipei, Taiwan 11529, Republic of China²Argonne National Laboratory, Argonne, Illinois 60439, USA

- ³University of Athens, 157 71 Athens, Greece
- ⁴Institut de Física d'Altes Energies, ICREA, Universitat Autònoma de Barcelona, E-08193, Bellaterra (Barcelona), Spain
- ⁵Baylor University, Waco, Texas 76798, USA
- ^{6a}Istituto Nazionale di Fisica Nucleare Bologna, I-40127 Bologna, Italy
- ^{6b}University of Bologna, I-40127 Bologna, Italy
- ⁷University of California, Davis, Davis, California 95616, USA
- ⁸University of California, Los Angeles, Los Angeles, California 90024, USA
- ⁹Instituto de Física de Cantabria, CSIC-University of Cantabria, 39005 Santander, Spain
- ¹⁰Carnegie Mellon University, Pittsburgh, Pennsylvania 15213, USA
- ¹¹Enrico Fermi Institute, University of Chicago, Chicago, Illinois 60637, USA
- ¹²Comenius University, 842 48 Bratislava, Slovakia and Institute of Experimental Physics, 040 01 Kosice, Slovakia
- ¹³Joint Institute for Nuclear Research, RU-141980 Dubna, Russia
- ¹⁴Duke University, Durham, North Carolina 27708, USA
- ¹⁵Fermi National Accelerator Laboratory, Batavia, Illinois 60510, USA
- ¹⁶University of Florida, Gainesville, Florida 32611, USA
- ¹⁷Laboratori Nazionali di Frascati, Istituto Nazionale di Fisica Nucleare, I-00044 Frascati, Italy
- ¹⁸University of Geneva, CH-1211 Geneva 4, Switzerland
- ¹⁹Glasgow University, Glasgow G12 8QQ, United Kingdom
- ²⁰Harvard University, Cambridge, Massachusetts 02138, USA
- ²¹Division of High Energy Physics, Department of Physics, University of Helsinki, FIN-00014, Helsinki, Finland and Helsinki Institute of Physics, FIN-00014 Helsinki, Finland
- ²²University of Illinois, Urbana, Illinois 61801, USA
- ²³The Johns Hopkins University, Baltimore, Maryland 21218, USA
- ²⁴Institut für Experimentelle Kernphysik, Karlsruhe Institute of Technology, D-76131 Karlsruhe, Germany
- ²⁵Center for High Energy Physics: Kyungpook National University, Daegu 702-701, Korea; Seoul National University, Seoul 151-742, Korea; Sungkyunkwan University, Suwon 440-746, Korea; Korea Institute of Science and Technology Information, Daejeon 305-806, Korea; Chonnam National University, Gwangju 500-757, Korea; Chonbuk National University, Jeonju 561-756, Korea; and Ewha Womans University, Seoul 120-750, Korea
- ²⁶Ernest Orlando Lawrence Berkeley National Laboratory, Berkeley, California 94720, USA
- ²⁷University of Liverpool, Liverpool L69 7ZE, United Kingdom
- ²⁸University College London, London WC1E 6BT, United Kingdom
- ²⁹Centro de Investigaciones Energéticas Medioambientales y Tecnológicas, E-28040 Madrid, Spain
- ³⁰Massachusetts Institute of Technology, Cambridge, Massachusetts 02139, USA
- ³¹University of Michigan, Ann Arbor, Michigan 48109, USA
- ³²Michigan State University, East Lansing, Michigan 48824, USA
- ³³Institution for Theoretical and Experimental Physics, ITEP, Moscow 117259, Russia
- ³⁴University of New Mexico, Albuquerque, New Mexico 87131, USA
- ³⁵The Ohio State University, Columbus, Ohio 43210, USA
- ³⁶Okayama University, Okayama 700-8530, Japan
- ³⁷Osaka City University, Osaka 558-8585, Japan
- ³⁸University of Oxford, Oxford OX1 3RH, United Kingdom
- ^{39a}Istituto Nazionale di Fisica Nucleare, Sezione di Padova, I-35131 Padova, Italy
- ^{39b}University of Padova, I-35131 Padova, Italy
- ⁴⁰University of Pennsylvania, Philadelphia, Pennsylvania 19104, USA
- ^{41a}Istituto Nazionale di Fisica Nucleare Pisa, I-56127 Pisa, Italy
- ^{41b}University of Pisa, I-56127 Pisa, Italy
- ^{41c}University of Siena, I-56127 Pisa, Italy
- ^{41d}Scuola Normale Superiore, I-56127 Pisa, Italy
- ^{41e}INFN Pavia, I-27100 Pavia, Italy
- ^{41f}University of Pavia, I-27100 Pavia, Italy
- ⁴²University of Pittsburgh, Pittsburgh, Pennsylvania 15260, USA
- ⁴³Purdue University, West Lafayette, Indiana 47907, USA
- ⁴⁴University of Rochester, Rochester, New York 14627, USA
- ⁴⁵The Rockefeller University, New York, New York 10065, USA
- ^{46a}Istituto Nazionale di Fisica Nucleare, Sezione di Roma 1, I-00185 Roma, Italy
- ^{46b}Sapienza Università di Roma, I-00185 Roma, Italy
- ⁴⁷Mitchell Institute for Fundamental Physics and Astronomy, Texas A&M University, College Station, Texas 77843, USA
- ^{48a}Istituto Nazionale di Fisica Nucleare Trieste, I-33100 Udine, Italy
- ^{48b}Gruppo Collegato di Udine, I-33100 Udine, Italy
- ^{48c}University of Udine, I-33100 Udine, Italy
- ^{48d}University of Trieste, I-34127 Trieste, Italy
- ⁴⁹University of Tsukuba, Tsukuba, Ibaraki 305, Japan

⁵⁰*Tufts University, Medford, Massachusetts 02155, USA*⁵¹*University of Virginia, Charlottesville, Virginia 22906, USA*⁵²*Waseda University, Tokyo 169, Japan*⁵³*Wayne State University, Detroit, Michigan 48201, USA*⁵⁴*University of Wisconsin, Madison, Wisconsin 53706, USA*⁵⁵*Yale University, New Haven, Connecticut 06520, USA*

(Received 26 August 2015; published 21 March 2016)

A measurement of vector boson (V) production in conjunction with a $D^*(2010)^+$ meson is presented. Using a data sample corresponding to 9.7 fb^{-1} of proton-antiproton collisions at center-of-mass energy $\sqrt{s} = 1.96 \text{ TeV}$ produced by the Fermilab Tevatron, we reconstruct $V + D^{*+}$ samples with the CDF II detector. The D^{*+} is fully reconstructed in the $D^*(2010)^+ \rightarrow D^0(\rightarrow K^-\pi^+)\pi^+$ decay mode. This technique is sensitive to the associated production of vector boson plus charm or bottom mesons. We measure the ratio of production cross sections $\sigma(W + D^*)/\sigma(W) = [1.75 \pm 0.13(\text{stat}) \pm 0.09(\text{stat})]\%$ and $\sigma(Z + D^*)/\sigma(Z) = [1.5 \pm 0.4(\text{stat}) \pm 0.2(\text{stat})]\%$ and perform a differential measurement of $d\sigma(W + D^*)/dp_T(D^*)$. Event properties are utilized to determine the fraction of $V + D^*(2010)^+$ events originating from different production processes. The results are in agreement with the predictions obtained with the PYTHIA program, limiting possible contribution from non-standard-model physics processes.

DOI: 10.1103/PhysRevD.93.052012

*Deceased.

^aVisitor from University of British Columbia, Vancouver, BC V6T 1Z1, Canada.^bVisitor from Istituto Nazionale di Fisica Nucleare, Sezione di Cagliari, 09042 Monserrato (Cagliari), Italy.^cVisitor from University of California Irvine, Irvine, CA 92697, USA.^dVisitor from Institute of Physics, Academy of Sciences of the Czech Republic, 182 21, Czech Republic.^eVisitor from CERN, CH-1211 Geneva, Switzerland.^fVisitor from Cornell University, Ithaca, NY 14853, USA.^gVisitor from University of Cyprus, Nicosia CY-1678, Cyprus.^hVisitor from Office of Science, U.S. Department of Energy, Washington, DC 20585, USA.ⁱVisitor from University College Dublin, Dublin 4, Ireland.^jVisitor from ETH, 8092 Zürich, Switzerland.^kVisitor from University of Fukui, Fukui City, Fukui Prefecture, Japan 910-0017.^lVisitor from Universidad Iberoamericana, Lomas de Santa Fe, México, C.P. 01219, Distrito Federal.^mVisitor from University of Iowa, Iowa City, IA 52242, USA.ⁿVisitor from Kinki University, Higashi-Osaka City, Japan 577-8502.^oVisitor from Kansas State University, Manhattan, KS 66506, USA.^pVisitor from Brookhaven National Laboratory, Upton, NY 11973, USA.^qVisitor from Istituto Nazionale di Fisica Nucleare, Sezione di Lecce, Via Arnesano, I-73100 Lecce, Italy.^rVisitor from Queen Mary, University of London, London, E1 4NS, United Kingdom.^sVisitor from University of Melbourne, Victoria 3010, Australia.^tVisitor from Muons, Inc., Batavia, IL 60510, USA.^uVisitor from Nagasaki Institute of Applied Science, Nagasaki 851-0193, Japan.^vVisitor from National Research Nuclear University, Moscow 115409, Russia.^wVisitor from Northwestern University, Evanston, IL 60208, USA.^xVisitor from University of Notre Dame, Notre Dame, IN 46556, USA.^yVisitor from Universidad de Oviedo, E-33007 Oviedo, Spain.^zVisitor from CNRS-IN2P3, Paris, F-75205 France.^{aa}Visitor from Universidad Tecnica Federico Santa Maria, 110v Valparaiso, Chile.^{bb}Visitor from Sejong University, Seoul 143-747, Korea.^{cc}Visitor from The University of Jordan, Amman 11942, Jordan.^{dd}Visitor from Universite catholique de Louvain, 1348 Louvain-La-Neuve, Belgium.^{ee}Visitor from University of Zürich, 8006 Zürich, Switzerland.^{ff}Visitor from Massachusetts General Hospital, Boston, MA 02114 USA.^{gg}Visitor from Harvard Medical School, Boston, MA 02114 USA.^{hh}Visitor from Hampton University, Hampton, VA 23668, USA.ⁱⁱVisitor from Los Alamos National Laboratory, Los Alamos, NM 87544, USA.^{jj}Visitor from Università degli Studi di Napoli Federico I, I-80138 Napoli, Italy.

In high-energy proton-antiproton ($p\bar{p}$) collisions, production of a vector boson, V , either a W^\pm or Z^0 boson, can occur in conjunction with one or more heavy quarks, Q , where $Q = c, b$. Standard model processes that contribute to $V + Q$ final states include direct (nonresonant) production as well as $V + Q$ final states originating from decays of top quarks and Higgs bosons. In addition, high mass, non-standard-model states could also contribute, and therefore a detailed study of $V + Q$ processes could be sensitive to these contributions.

In the standard model, production and decay of $V + Q$ states is governed by a combination of the strong and weak interactions. For example, the $p\bar{p} \rightarrow W + c$ process is sensitive to the magnitude of the Cabibbo-Kobayashi-Maskawa matrix element V_{cs} as well as the strange quark distribution function of the proton [1,2]. Measurements of this process, along with the related processes $V + b\bar{b}$ and $V + c\bar{c}$, can be used in conjunction with our knowledge of the weak interaction in order to test our understanding of the strong interaction at high energy [3]. Study of these processes also helps to provide better modeling of the backgrounds relevant to non-standard-model searches at the Tevatron and LHC.

Previous Tevatron analyses of $p\bar{p} \rightarrow V + c$ production have measured the absolute and relative cross sections $\sigma(V + c)/\sigma(V + \text{jets})$ [4–7]. Restrictions on jet acceptance along with the heavy flavor identification techniques limited these analyses to high-momentum ($p_T(\text{jet}) \gtrsim 20 \text{ GeV}/c$) charm and bottom hadrons. In addition, systematic uncertainties arose in the inclusive tagging techniques used to separate light-quark, gluon, and heavy-quark contributions. Similar measurements have been carried out at the LHC [8–10].

Here, we present a complementary technique in which the charm decay is fully reconstructed as a $D^*(2010)^+$ meson (denoted as D^{*+}) through the decay chain $D^{*+} \rightarrow D^0\pi_s^+$ followed by $D^0 \rightarrow K^-\pi^+$ [11]. The subscript on π_s is used to denote a “soft” pion with low average momentum compared to the other pion arising from the D^0 decay. This full charm reconstruction provides additional information (charge correlation between decay products, impact parameter) to further classify signal contributions. With this identification technique, an improved measurement range of transverse momentum $p_T(D^{*+}) > 3 \text{ GeV}/c$ is achieved, with an average value of $10 \text{ GeV}/c$. In addition to $V + c$, the sample identified with this technique contains contributions from $V + c\bar{c}$ and charm from the sequential decay of the $V + b\bar{b}$ process. Full reconstruction of charmed final states in W boson events has been carried out at the LHC [9].

In reconstructing low-momentum charm hadrons in vector boson events, this work isolates a data sample that has been previously unexplored. To date, anomalous charm hadron production in $p\bar{p}$ collisions, particularly at low $p_T(c)$, has not been ruled out. By isolating and quantifying a unique set of $V + c$ events, this analysis constitutes a new test of the standard model.

This work utilizes the full data set collected by the CDF II detector at the Fermilab Tevatron collider, with an integrated luminosity of 9.7 fb^{-1} for $p\bar{p}$ collisions at $\sqrt{s} = 1.96 \text{ TeV}$. The CDF II detector [12] is a general-purpose magnetic spectrometer surrounded by a projective-tower calorimeter and a muon detector. The CDF II central tracking volume consists of a silicon detector surrounded by a large open-cell drift chamber. The entire tracking volume is contained within a uniform axial magnetic field parallel to the proton beam direction [13].

Events are selected with a three-level online event selection system (trigger). This analysis considers events selected by an inclusive high- p_T lepton trigger requiring an electron (muon) with $E_T > 18 \text{ GeV}$ ($p_T > 18 \text{ GeV}/c$) [13]. From this high- p_T lepton data set, we select vector-boson events as described below.

A Z^0 candidate is required to have two oppositely-charged, isolated electrons (muons), each with $E_T > 25 \text{ GeV}$ ($p_T > 20 \text{ GeV}/c$) and $|\eta| < 1.1$. A lepton is considered isolated if $I < 0.1$, where I is the isolation, defined as ratio of the total transverse energy in a cone of radius $\Delta R \equiv \sqrt{\Delta\phi^2 + \Delta\eta^2} = 0.4$ about the lepton track (excluding the lepton) with respect to $E_T(p_T)$ of the electron (muon). The invariant mass of the lepton pair $m(\ell^+\ell^-)$ is required to fall between 66 and $116 \text{ GeV}/c^2$. Background in the Z^0 candidate sample is estimated by fitting the invariant mass distribution to a double-Gaussian signal plus an exponential background hypothesis. The number of signal events is obtained by integrating the double-Gaussian distribution, yielding 241450 ± 580 (257580 ± 550) $Z^0 \rightarrow ee(\mu\mu)$ events, where the uncertainty is statistical only. The dilepton data and fits are shown in Fig. 1.

A candidate W^+ event is required to have missing transverse energy $\cancel{E}_T > 25(20) \text{ GeV}$ [14], one isolated electron (muon) with $E_T > 25 \text{ GeV}$ ($p_T > 20 \text{ GeV}/c$) and pseudorapidity $|\eta| < 1.1$. Missing transverse energy is corrected for muons and other instrumental effects that may produce false \cancel{E}_T . Finally, the transverse mass of the W , $M_T = \sqrt{2E_T\cancel{E}_T(1 - \cos\Delta\phi)}$, where E_T is the transverse energy of the lepton and $\Delta\phi$ is the azimuthal angle between the lepton and missing transverse energy, must satisfy $M_T > 20 \text{ GeV}/c^2$.

Background to the W candidates consists of electroweak sources ($Z \rightarrow \ell^+\ell^-$ and $W \rightarrow \tau\nu$ events, denoted as EWK hereafter) and from hadrons displaying a similar topology as W events (multijet background). We estimate the number of all such background events by first relaxing the selection criteria on lepton I and event \cancel{E}_T and then defining four regions A, B, C, and W in the \cancel{E}_T/I plane (Table I). Region W is the signal region as defined earlier, while the other regions contain primarily multijet events mimicking the W signature. Lepton isolation versus missing transverse energy is shown in Fig. 2.

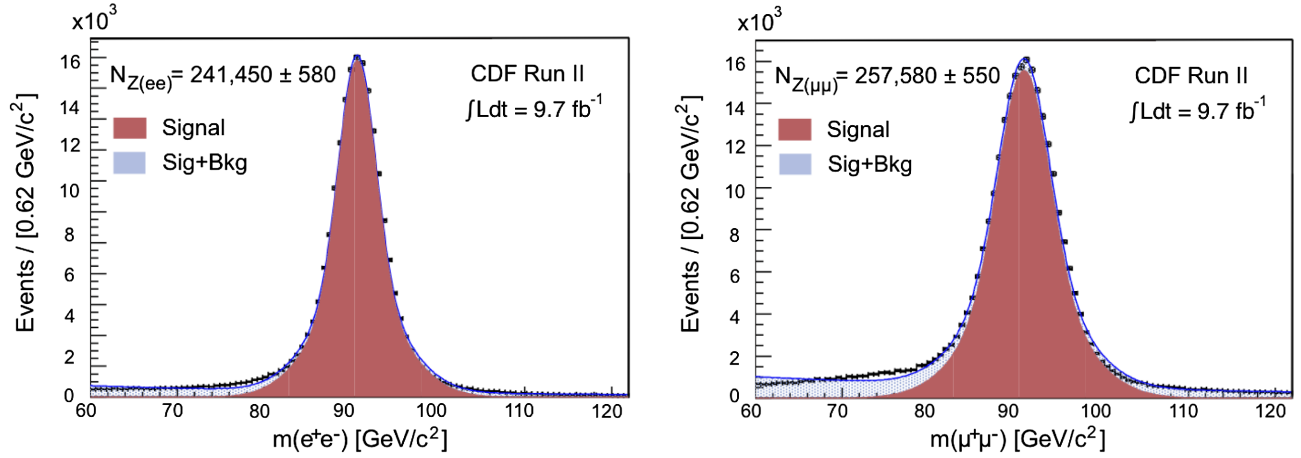


FIG. 1. Distribution of dielectron (left) and dimuon (right) invariant mass. The fit to the data is described in the text.

We estimate $N_{\text{jet}}^W = N_{\text{jet}}^C \times N_{\text{jet}}^A / N_{\text{jet}}^B$, where N_{jet}^X is the number of multijet events in region X , as done in Ref. [15]. The contamination arising from EWK and residual signal events in regions A, B, and C is estimated using the PYTHIA 6.2 Monte Carlo simulation [16]. The simulation is used to predict the backgrounds relative to the yield of $W \rightarrow \ell\nu$ events in signal region W. By relating other contributions to the number of signal events, we produce a system of linear equations to be solved for the number of $W \rightarrow \ell\nu$ signal events in region W. The solutions determine the contribution of each background in each region. Of 5081938 (5348975) candidate events in region W, 93.6 (91.5)% are $W \rightarrow e\nu(\mu\nu)$ signal. Uncertainties in these estimates are considered later in the determination of fractions $N(W + D^{*+})/N(W)$.

For all W and Z candidate events, we search for D^{*+} mesons by considering all reconstructed charged particles (tracks) within 2.0 cm longitudinally of the point of closest approach of the high- p_T lepton to the beamline ($|\Delta z| < 2.0$ cm). For each possible set of three tracks with unit total net charge, we hypothesize a match to the $D^{*+} \rightarrow D^0(\rightarrow K^-\pi^+)\pi_s^+$ decay mode and test for consistency. To ensure well-measured tracks, each track must satisfy $|\eta| < 1.1$, and $p_T(K)$ and $p_T(\pi) > 400$ MeV/ c , $p_T(\pi_s) > 80$ MeV/ c . We also require $\Delta R < 1.1$ for each pair of tracks. As $D^0 \rightarrow K^-\pi^+$ is CKM-favored versus $D^0 \rightarrow K^+\pi^-$ by a factor of 10^4 , the two pions are required to have the same charge.

The resulting sample is subjected to a kinematic fit to reconstruct D^{*+} and D^0 vertices from the K , π and π_s track

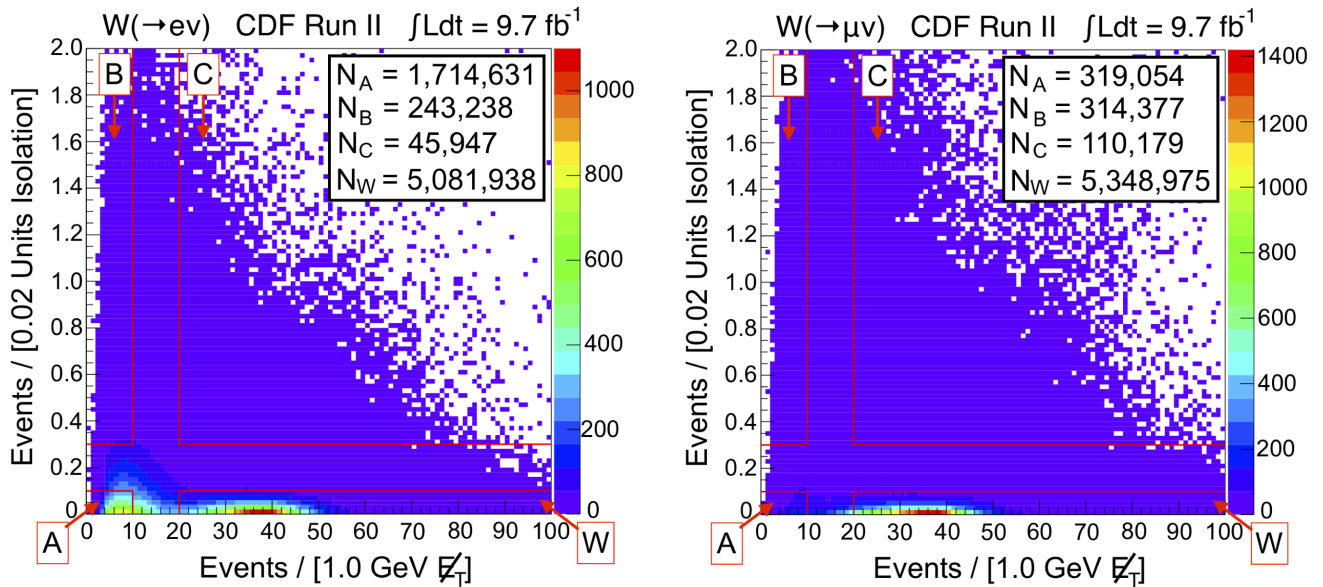


FIG. 2. Lepton isolation versus missing transverse energy for electron (left) and muon (right) events passing the selection criteria described in the text. The regions identified in Table I are shown graphically on the plots. The W signal is dominant in the region $I < 0.05$ and $20 < E_T < 50$ GeV/ c .

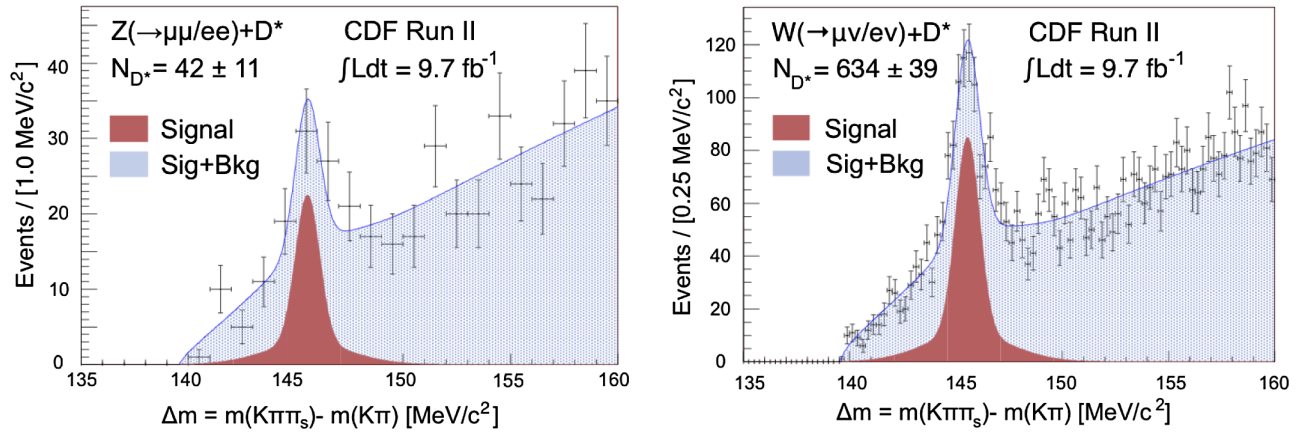


FIG. 3. Distribution of mass difference between the D^{*+} and D^0 candidates in Z and W events, with fit results overlaid. The electron and muon decay modes are combined.

candidates. The K and π candidates must intersect to form a candidate D^0 vertex, and the D^0 candidate must intersect with the π_s to form a D^{*+} vertex. Since direct charm (e.g., $p\bar{p} \rightarrow Wc$, $p\bar{p} \rightarrow Wc\bar{c}$) as well as indirect charm (e.g., $Wb\bar{b}$ with $b \rightarrow c$) are of interest, the trajectory of the reconstructed D^{*+} is not required to point back to the primary $\bar{p}p$ vertex. Finally, we require the D^0 mass, determined by the fit, to fall within $3\sigma = 0.033 \text{ GeV}/c^2$ of the known D^0 mass value, $m_{D^0} = 1.865 \text{ GeV}/c^2$ [17].

To reduce background in the D^{*+} selection, we train an artificial neural network (ANN) to discriminate among D^{*+} candidates using 19 variables as described in chapter 5 of Ref. [18]. These variables include charged-particle momenta and opening angles; the distance between the $p\bar{p}$ collision vertex and the reconstructed D^{*+} and D^0 vertices; and track impact parameters. To train the ANN, we provide samples of signal and background events. For signal, we generate a sample of $W + D^{*+}$ events using PYTHIA 6.2 [16] followed by a full detector simulation. For ANN training, we define the signal sample as all simulated $W + D^{*+}$ candidates with mass difference, $\Delta m \equiv m(K\pi\pi_s) - m(K\pi)$, within $3\sigma = 0.0029 \text{ GeV}/c^2$ of the known mass-difference value $\Delta m(D^{*+} - D^0) = 0.1455 \text{ GeV}/c^2$ [17]. To model background for ANN training, we choose D^{*+} candidates in data that pass all fitting and kinematic selection criteria, but whose final-state particles do not have the proper sign correlations (e.g., $K^-\pi^-\pi_s^+$). To model background events as accurately as possible, we require these background D^{*+} candidates to fall within 3.2σ of the peak, a compromise that allows an equal number of signal and background events for optimal ANN training. Control data samples as well as simulated samples are utilized to verify that the ANN is well behaved and unbiased [18].

We map ANN output scores to the region $[-1.0, 1.0]$, with more positive numbers being more signal-like. Candidates are required to have an ANN score greater than 0.0 to be classified as signal. This suppresses 80% of the background while retaining 90% of the signal.

With this algorithm, we search the selected vector-boson-candidate events for D^{*+} candidates. To measure the D^{*+} yield, we fit the Δm distribution to a power-law background plus double-Gaussian signal hypothesis. We use a template for the double-Gaussian signal, taken from a fit to simulated signal events, with the signal width increased by a factor of 1.1. This accounts for the slightly better mass resolution observed in the simulation [18].

We obtain the following yields in the W candidate sample: $N(W(e\nu) + D^{*+}) = 340 \pm 30$ and $N(W(\mu\nu) + D^{*+}) = 294 \pm 26$, where the uncertainties are statistical only. In the Z candidate sample, we observe $N(Z(ee) + D^{*+}) = 22 \pm 9$ and $N(Z(\mu\mu) + D^{*+}) = 20 \pm 7$ events. When the electron and muon decay channels are combined, the yields are $N(W(\mu\nu/ev) + D^{*+}) = 634 \pm 39$ and $N(Z(\mu\mu/ee) + D^{*+}) = 42 \pm 11$. The mass-difference distributions are shown in Fig. 3. Yields reported here are the number of reconstructed D^{*+} in events passing V candidate selection criteria, and therefore represent the number of reconstructed D^{*+} produced in conjunction with both signal and background V candidates. In the following, we account for the background V contribution in $V + D^{*+}$ candidate events.

For Z candidates, we define two regions in $\ell^+\ell^-$ mass: The signal region is defined as $|m_{\ell^+\ell^-} - 91 \text{ GeV}/c^2| \leq 3\sigma$, and the background region is defined as $|m_{\ell^+\ell^-} - 91 \text{ GeV}/c^2| > 3\sigma$, with $\sigma = 2.0(3.0) \text{ GeV}/c^2$ for $Z \rightarrow \mu\mu(ee)$ bounded by the $66 < m_{\ell^+\ell^-} < 116 \text{ GeV}/c^2$ mass window. We fit the m_Z distribution to a double-Gaussian signal plus exponential background hypothesis, and integrate beneath the curves to estimate the signal and background yields in each region. For each region, we fit the Δm for all D^{*+} candidates using our previously defined signal plus background fitting function. This provides D^{*+} yields in the signal and background regions. Two coupled linear equations are used to solve for the rates $f_{D^{*+}}^{Z,\text{sig}}$ ($f_{D^{*+}}^{Z,\text{bkg}}$) at which signal (background) Z candidates are produced with D^{*+} mesons as described in chapter 6 of Ref. [18].

After measuring these rates, the procedure is repeated for various choices of signal and background $m(\ell^+\ell^-)$ boundaries. We fit the set of all $f_{D^{*+}}^{Z,\text{sig}}$ values found using these definitions to a constant value hypothesis, and take the variation in this fit to be the systematic uncertainty due to the unknown rate of D^{*+} mesons produced in association with V backgrounds. This is done separately for $Z \rightarrow e^+e^-$ and $\mu^+\mu^-$ decay channels, giving a systematic uncertainty in $f_{D^{*+}}^{Z,\text{sig}}$ of 20% for the $Z \rightarrow \mu\mu$ channel, and of 11% for the $Z \rightarrow ee$ channel.

To determine the number of real V plus real D^{*+} events, we follow a procedure similar to that outlined above to determine the background contributions to the W sample. We split candidate events into E_T/I regions A, B, C, and W, as defined in Table I. Each region contains D^{*+} mesons produced with signal W , as well as D^{*+} produced with three background sources: $W \rightarrow \tau\nu$, $Z \rightarrow \ell^+\ell^-$, and multijet events. The linear equations are solved simultaneously for the rates $f_{D^{*+}}^{W,\text{sig}}$ ($f_{D^{*+}}^{W,\text{bkg}}$) at which signal (background) W candidates are produced with D^{*+} mesons (see Sec. VI.3 of Ref. [18].) The associated systematic uncertainty is determined by repeating the procedure for several definitions of regions A, B, C and W, first keeping the I boundaries fixed and varying the E_T boundaries, and then keeping the E_T boundaries fixed and varying the I boundaries. This is done separately for the electron and muon W decay channels. The resulting systematic uncertainty in $f_{D^{*+}}^W$ is 10% in the $W \rightarrow e\nu$ channel, and 2% in the $W \rightarrow \mu\nu$ channel. The larger uncertainty for the $W(\rightarrow e\nu)$ case is due to a larger fraction of multijet background, relative to the $W \rightarrow \mu\nu$ case.

The full results of the sample composition studies are reported in chapter 6 of Ref. [18]. We observe the rate of D^{*+} mesons produced in events with falsely reconstructed V bosons to be considerably higher than the rate of D^{*+} mesons observed in real V events. This arises through Quantum Chromodynamic (QCD) processes producing falsely reconstructed leptons.

We unfold tagged signal fractions, $f_{D^{*+}}^V$, to ratios $\sigma(V + D^{*+})/\sigma(V)$, where $V = (W, Z)$, by following the prescription

TABLE I. Boundaries used to define regions A, B, C, and W for W candidates in the E_T - I plane. Regions A, B, and C consist primarily of multijet background and are used to estimate the multijet background content of signal region W. Numbers in parentheses are for $W^+ \rightarrow \mu^+\nu$ when different from the $W^+ \rightarrow e^+\nu$ boundaries.

Region	E_T range	I range
A	< 10 GeV	< 0.1
B	< 10 GeV	> 0.3
C	$> 25(20)$ GeV	> 0.3
W	$> 25(20)$ GeV	< 0.1

$$\frac{\sigma(V + D^{*+})}{\sigma(V)} = \frac{f_{D^{*+}}^V (A \cdot \epsilon)_V}{(A \cdot \epsilon)_{V+D^{*+}} \mathcal{B}(D^{*+} \rightarrow D^0(\rightarrow K\pi)\pi_s)} \quad (1)$$

Here, the branching ratio $\mathcal{B}(D^{*+} \rightarrow D^0(\rightarrow K\pi)\pi_s)$ is 0.0263 ± 0.0004 [17], and $(A \cdot \epsilon)_V$, $(A \cdot \epsilon)_{V+D^{*+}}$ is our total (geometric plus kinematic) acceptance for V and $V + D^{*+}$ events, respectively.

To determine the V acceptances, we apply the W/Z tagging algorithms over inclusive simulated samples generated using PYTHIA 6.2. For the $V + D^{*+}$ acceptances, we determine the values of $(A \cdot \epsilon)$ both differentially as a function of $p_T(D^{*+})$, and for the inclusive set of all events with $p_T(D^{*+}) > 3$ GeV, the threshold below which the analysis acceptance vanishes. In the differential case, bins are chosen such that the expected number of tagged D^{*+} candidates in each bin is approximately constant according to simulation. Bins are as shown in Fig. 4; refer to chapter 8 of Ref. [18] for specific values.

Systematic uncertainties on the production cross sections arise from sample yield and purity estimates, acceptance, efficiency, and simulation [18]. Sources of uncertainty that

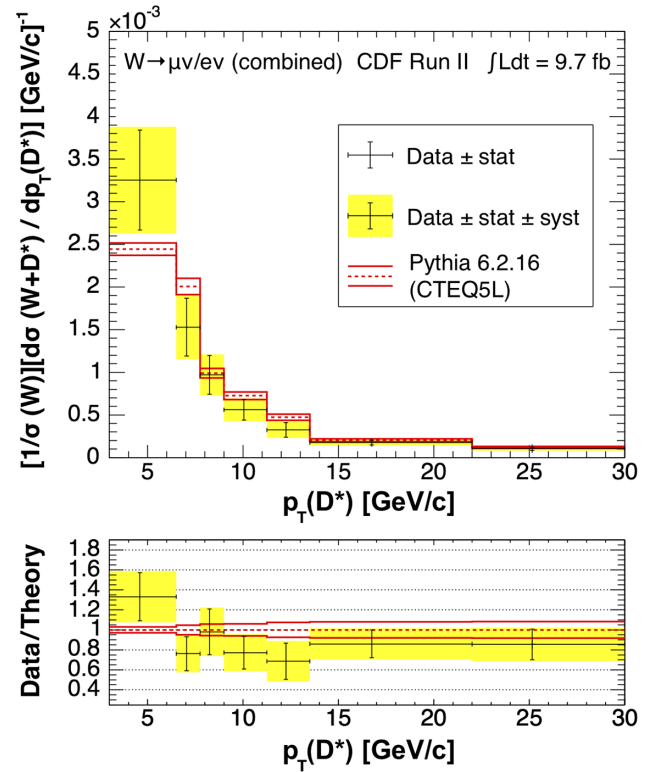


FIG. 4. Ratio of cross sections $\sigma(W + D^{*+})/\sigma(W)$ as a function of $p_T(D^{*+})$, for combined $W \rightarrow e\nu$ and $W \rightarrow \mu\nu$ results. Error bars show the statistical uncertainty; the sum in quadrature of the statistical and systematic errors is shown as a yellow error band. The dotted red line shows the prediction of PYTHIA 6.2 obtained using the CTEQ5L PDF, with solid red lines showing PDF uncertainty in this prediction. The ratio of the simulated distribution to data is shown in the lower plot.

TABLE II. Ratio of cross sections $\sigma(V + D^{*+})/\sigma(V)$ for the inclusive sample $p_T(D^{*+}) > 3$ GeV/ c , and predictions of PYTHIA 6.2.16 simulation using the CTEQ5L PDF. For results from data, the first uncertainty is statistical, the second is systematic. For results from simulation, uncertainty listed is statistical.

Sample	$\sigma(V + D^{*+})/\sigma(V)$ (in %)	
	Data	PYTHIA 6.2.16
$W \rightarrow e\nu$	$1.74 \pm 0.21 \pm 0.17$	
$W \rightarrow \mu\nu$	$1.75 \pm 0.17 \pm 0.05$	1.77 ± 0.07
W combined	$1.75 \pm 0.13 \pm 0.09$	
$Z^0 \rightarrow ee$	$1.0 \pm 0.6 \pm 0.2$	
$Z^0 \rightarrow \mu\mu$	$1.8 \pm 0.5 \pm 0.2$	1.36 ± 0.05
Z^0 combined	$1.5 \pm 0.4 \pm 0.2$	

are common in measurements of total cross section (e.g., luminosity and trigger efficiency uncertainties), cancel when taking the ratio $\sigma(V + D^{*+})/\sigma(V)$.

The systematic uncertainty in $(A \cdot \epsilon)$ is dominated by the uncertainty in the CTEQ [19] parton-distribution function (PDF) of the proton chosen for this analysis. Uncertainties due to the PDFs are estimated using 90% confidence-level (C.L.) variations on the 20 CTEQ eigenvectors. To investigate possible further dependencies on the chosen PDF, the MSTW2008 [20] central value is also checked. When the difference between CTEQ and MSTW2008 is smaller than the uncertainty from variations on the 20 eigenvectors, no additional uncertainty is taken. When the difference is larger, that difference is added in quadrature to the eigenvector uncertainty. Uncertainty in $\alpha_s(M_Z)$ at 90% C.L. is taken as an additional systematic uncertainty, and added in quadrature to the above.

For both the W and Z samples, we find the ratio $\sigma(V + D^{*+})/\sigma(V)$ for the inclusive set of events $p_T(D^{*+}) > 3$ GeV/ c . For the W samples only, we unfold $f_{D^{*+}}^W$ differentially as a function of $p_T(D^{*+})$. Results from the electron and muon decay channels are combined using a best-linear-uncertainty estimator, assuming that systematic uncertainties are fully correlated across W or Z decay modes. The final results are shown in Table II and Fig. 4, and in all cases agree with the PYTHIA predictions within uncertainties.

The $W + D^{*+}$ signal events are expected to come from three different production processes: $s(d) + g \rightarrow W + c$ (Wc), $q + \bar{q}' \rightarrow W + g(\rightarrow c\bar{c})$ (Wcc), and $q + \bar{q}' \rightarrow W + g(\rightarrow b\bar{b})$ (Wbb). Due primarily to a difference in $p_T(D^{*+})$ spectra, a neural network may generally identify D^{*+} from different sources (Wcc , Wc , and Wbb) with different efficiencies. This enables the fraction of signal from each production process to be determined.

We train two tiers of neural networks; the first consists of networks that are trained to identify one type of signal (Wcc , Wc , and Wbb) versus the D^{*+} background sample described earlier; the second consists of networks that are

trained to identify one type of signal over another (Wcc vs Wbb , Wc vs Wcc , and Wbb vs Wc). Each first-tier neural network is paired with a second-tier neural network, in order to select D^{*+} candidates from one production source preferentially, over all other D^{*+} candidates as described in chapter 10 of Ref. [18]. We apply each ANN-pair to simulated signal events to determine the efficiencies with which each pair identifies D^{*+} from each production source, obtaining a matrix of efficiencies. We finally apply each ANN-pair to the data and determine three yields. We solve the resulting linear equations to find fractions X^{Wc} , X^{Wcc} , and X^{Wbb} , where X^Y is the fraction of $W + D^{*+}$ signal that comes from production process Y . After repeating the technique by varying the efficiencies for each process, we determine that the uncertainty is dominantly statistical.

This method gives good separation for X^{Wbb} , but is not very effective at determining the fraction X^{Wc} owing to similarities in the kinematic properties of D^{*+} from Wcc , and from Wc . In the case of Wc production, conservation of charge requires that the W and D^{*+} are produced with opposite signs. In Wcc or Wbb production, however, we are equally likely to identify oppositely charged W and D^{*+} , $(W + D^{*+})_{OS}$, or same-signed W and D^{*+} , $(W + D^{*+})_{SS}$. We therefore determine the number of Wc events in the $W + D^{*+}$ signal by taking the difference $(W + D^{*+})_{OS} - (W + D^{*+})_{SS}$. We divide by the sum $(W + D^{*+})_{OS} + (W + D^{*+})_{SS}$ to get the fraction X^{Wc} . The uncertainty in this measurement of X^{Wc} is statistical only and treated as uncorrelated with the uncertainty in the measurement of X^{Wbb} , due to the use of a different technique for finding each fraction. Normalized to unity, the production-process fractions in the overall $W + D^{*+}$ signal are obtained as $X^{Wcc} = 73 \pm 8\%$, $X^{Wbb} = 13 \pm 5\%$, $X^{Wc} = 14 \pm 6\%$. The relative contribution of these processes is momentum dependent. In particular, our ability to identify low-momentum D^{*+} candidates enhances the Wcc contribution compared to analyses performed at higher momenta [18].

In conclusion, we present the first measurement of $V + D^{*+}$ production at hadron colliders in the regime $p_T(D^{*+}) > 3$ GeV/ c . The expected rate of D^{*+} production in V events is as predicted by PYTHIA 6.2, both for the integrated sample $p_T(D^{*+}) > 3$ GeV/ c , and differentially as a function of $p_T(D^{*+})$.

We thank the Fermilab staff and the technical staffs of the participating institutions for their vital contributions. This work was supported by the U.S. Department of Energy and National Science Foundation; the Italian Istituto Nazionale di Fisica Nucleare; the Ministry of Education, Culture, Sports, Science and Technology of Japan; the Natural Sciences and Engineering Research Council of Canada; the National Science Council of the Republic of China; the Swiss National Science Foundation; the A. P. Sloan

Foundation; the Bundesministerium für Bildung und Forschung, Germany; the Korean World Class University Program, the National Research Foundation of Korea; the Science and Technology Facilities Council and the Royal Society, United Kingdom; the Russian Foundation for

Basic Research; the Ministerio de Ciencia e Innovación, and Programa Consolider-Ingenio 2010, Spain; the Slovak R&D Agency; the Academy of Finland; the Australian Research Council (ARC); and the EU community Marie Curie Fellowship Contract No. 302103.

-
- [1] H. L. Lai, P. Nadolsky, J. Pumplin, D. Stump, W. K. Tung, and C.-P. Yuan, *J. High Energy Phys.* **04** (2007) 089.
- [2] U. Baur, F. Halzen, S. Keller, M. Mangano, and K. Riesselmann, *Phys. Lett. B* **318**, 544 (1993).
- [3] W. T. Giele, S. Keller, and E. Laenen, *Phys. Lett. B* **372**, 141 (1996).
- [4] T. Aaltonen *et al.* (CDF Collaboration), *Phys. Rev. Lett.* **100**, 091803 (2008).
- [5] T. Aaltonen *et al.* (CDF Collaboration), *Phys. Rev. Lett.* **110**, 071801 (2013).
- [6] V. M. Abazov *et al.* (D0 Collaboration), *Phys. Lett. B* **666**, 23 (2008).
- [7] V. M. Abazov *et al.* (D0 Collaboration), *Phys. Rev. Lett.* **112**, 042001 (2014).
- [8] S. Chatrchyan *et al.* (CMS Collaboration), *J. High Energy Phys.* **02** (2014) 013.
- [9] G. Aad *et al.* (ATLAS Collaboration), *J. High Energy Phys.* **05** (2014) 068.
- [10] R. Aaij *et al.* (LHCb Collaboration), *Phys. Rev. D* **92**, 052001 (2015); *J. High Energy Phys.* **02** (2014) 013.
- [11] Charge conjugate modes are implied throughout unless specifically noted.
- [12] D. Acosta *et al.* (CDF Collaboration), *Phys. Rev. D* **71**, 032001 (2005).
- [13] A coordinate system is used with the z axis along the proton beam direction; θ is the polar angle, ϕ is the azimuthal angle, pseudorapidity is $\eta = -\ln[\tan(\theta/2)]$, transverse momentum is $p_T = |p| \sin \theta$, and transverse energy is $E_T = E \sin \theta$.
- [14] The missing transverse energy, \cancel{E}_T , is defined as the magnitude of the energy imbalance as measured in the calorimeter, $\cancel{E}_T = |-\sum \vec{E}_T|$. The \cancel{E}_T is corrected for calorimeter geometry, highly penetrating muons and other instrumental effects.
- [15] A. Abulencia *et al.* (CDF Collaboration), *J. Phys. G* **34**, 2457 (2007).
- [16] S. Mrenna, T. Sjöstrand, and P. Skands, *J. High Energy Phys.* **05** (2006) 026.
- [17] J. Beringer *et al.* (Particle Data Group), *Phys. Rev. D* **86**, 010001 (2012).
- [18] K. Matera, Ph.D. thesis, University of Illinois, Report No. FERMILAB-THESIS-2014-17.
- [19] J. Pumplin, D. R. Stump, J. Huston, H. L. Lai, P. M. Nadosky, and W. K. Tung, *J. High Energy Phys.* **07** (2002) 012; D. Stump, J. Huston, J. Pumplin, W. K. Tung, H. L. Lai, S. Kuhlmann, and J. F. Owens, *J. High Energy Phys.* **10** (2003) 046.
- [20] A. D. Martin, W. J. Stirling, R. S. Thorne, and G. Watt, *Eur. Phys. J. C* **63**, 189 (2009).